

OPEN

Preoperative CT texture features predict prognosis after curative resection in pancreatic cancer

Hyung Sun Kim¹, Young Jae Kim², Kwang Gi Kim^{2*} & Joon Seong Park^{1*}

Pancreatic cancer is a lethal disease, and resistance to chemotherapy is a critical factor influencing the postoperative prognosis. Tumour heterogeneity is an important indicator of chemoresistance. Therefore, we analysed tumour heterogeneity in preoperative computed tomography scans by performing texture analysis using the grey-level run-length matrix and analysed the correlation of survival with the value obtained in these analyses. We analysed 116 consecutive patients who underwent curative resection and had preoperative contrast-enhanced computed tomography data available for analysis. A region of interest was drawn on all slices with a visible tumour and normal pancreas on the arterial phase computed tomography scans; the correlation of pathological characteristics with grey-level run-length matrix features was analysed. We then performed Kaplan–Meier survival curve analysis among pancreatic cancer patients. The grey-level non-uniformity values in grey-level run-length matrix features for tumours were higher than those for normal pancreas. High grey-level non-uniformity values represent a non-uniform texture, i.e., heterogeneity. Grey-level run-length matrix features showed that recurrence-free survival was shorter in the group with high grey-level non-uniformity 135 values ($p = 0.025$). Our analyses of the correlation between pathological outcomes and grey-level run-length matrix features in pancreatic cancer patients showed that grey-level non-uniformity values were powerful prognostic indicators.

Pancreatic cancer is a lethal disease with 2-year metastasis and recurrence rates of 80% even in patients who undergo curative resection because of resistance to chemotherapy^{1,2}. Chemoresistance is an important factor influencing the prognosis after curative resection, and tumour heterogeneity is an important indicator of the chemoresistance. Although other studies are underway to predict the prognosis or to characterise cancer phenotypes^{3,4}, image texture analysis is currently used to predict tumour heterogeneity. In this regard, several studies have reported the correlation between tumour heterogeneity and the prognosis in oesophageal cancer, lung cancer, and cervical cancer^{5–8}. However, only a few studies have reported texture analyses of tumour heterogeneity in pancreatic cancer⁹.

Texture analyses employ several methods, such as grey-level co-occurrence matrix (GLCM) and histogram analyses, to calculate or classify objects based on their texture. By assessing the distribution of grey levels, coarseness, and regularity within a lesion, computed image analysis algorithms can provide additional morphological information related to tumour heterogeneity. These texture analyses also offer the advantage of quantifying tumour heterogeneity, which cannot be reliably achieved by simple visual analysis. Therefore, in this study, we analysed tumour heterogeneity using preoperative computed tomography (CT) by performing texture analysis with the grey-level run-length matrix (GLRLM) approach. We then used these data to analyse the correlation between survival and the obtained tumour heterogeneity values in a large sample of curative-intent resected pancreatic cancers.

Results

Clinical characteristics of the patients with pancreatic cancer. Table 1 shows the patient characteristics in this study. The median age of the patients was 65.0 years, and the study population included 56 men (48.3%). In the T stage classification (American Joint Committee on Cancer (AJCC) 8th edition¹⁰), 21 (18.1%) patients had T1 stage disease; 77 patients (66.4%), T2 stage disease; and 18 (15.5%) patients, T3 stage disease. In

¹Pancreatobiliary Cancer Clinic, Department of Surgery, Gangnam Severance Hospital, Yonsei University, Seoul, Korea. ²Department of Biomedical Engineering, Gachon University College of Medicine, Incheon, Korea. *email: kimkg@gachon.ac.kr; JSPARK330@yuhs.ac

Age		Median [Q1–Q3] or N (%)
		65.0 [55.75–70.25]
Sex	Men	56 (48.3%)
	Women	60 (51.7%)
T stage (8 th)	T1	21 (18.1%)
	T2	77 (66.4%)
	T3	18 (15.5%)
N stage (8 th)	N0	42 (36.2%)
	N1	55 (47.4%)
	N2	19 (16.4%)
Stage (8 th)	IA	12 (10.3%)
	IB	22 (18.9%)
	IIA	8 (7%)
	IIB	55 (47.4%)
	III	19 (16.4%)
PNI	Positive	98 (84.5%)
	Negative	17 (14.6%)
	Unknown	1 (0.9%)
LVI	Positive	57 (49.1%)
	Negative	58 (50%)
	Unknown	1 (0.9%)
Differentiation	WD	10 (8.6%)
	MD	92 (79.3%)
	PD	13 (11.2%)
	Unknown	1 (0.9%)

Table 1. Pathological characteristics in pancreatic cancer patients. PNI; Perineural invasion, LVI; Lymphovascular invasion, WD; Well differentiated, MD; Moderate differentiated, PD; Poorly differentiated.

the N stage classification (AJCC 8th edition), 42 (36.2%) patients had N0 stage disease; 55 (47.4%) patients, N1 stage disease; and 19 (16.4%) patients, N2 stage disease. Perineural invasion was observed in 98 patients (84.5%), while lymphovascular invasion was observed in about half of the patients (n = 57, 49.1%). Most patients showed moderate differentiation (n = 92, 79.3%)

GLRLM features and their correlation with pathological characteristics. Texture analysis was performed using ROIs (region of interests) of the same size in the arterial phase images of preoperative CT scans. The GLN (Grey-level non-uniformity) values for GLRLM features in the tumour were higher than those for the normal pancreas (median value of GLN0, GLN45, and GLN90 in normal tissues = 0.0543; GLN135 in normal tissues = 0.055; median value of GLN0, GLN45, and GLN90 in the tumour = 0.0553; GLN135 in the tumour = 0.0563).

Tables 2 and 3 show the results for the GLN features. Table 2 shows the results for GLN0, GLN45, and GLN90, indicating significant differences in the T stage. The proportion of cases with stage T3 disease was higher in the group with values higher than the median than in the group with values lower than the median (p = 0.046). The proportion of poorly differentiated tumours was higher in the group with values higher than the median (p = 0.054). For GLN135, there were no significant factors except the T stage and differentiation (Table 3). The proportion of cases with stage T3 disease and poorly differentiated tumours was higher in the group with values higher than median.

Survival analysis. The GLN values were used to create a Kaplan–Meier survival curve. Recurrence-free survival was shorter in the group with high GLN135 values (p = 0.025) (median recurrence-free survival: group with values higher than the median = 6.72 months, group with values lower than the median = 10.52 months). As described above, GLN indicates heterogeneity. This result showed that a high GLN135 value was associated with a poor prognosis (Fig. 1).

Prognostic impact of clinicopathologic features in pancreatic cancer. On multivariate analyses, node stage, tumour differentiation, and GLN135 value were identified as independent factors for poor recurrence-free survival (Table 4).

Prognostic impact of clinicopathologic features in pancreatic cancer. On multivariate analyses, tumour stage, tumour differentiation, and perineural invasion were identified as independent factors for poor overall survival (Table 5).

		GLN 0,45,90		p-value
		Value < Median (n = 48)	Value > Median (n = 68)	
Age	≤65	28 (58.3%)	31 (45.6%)	0.176
	>65	20 (41.7%)	37 (54.4%)	
Sex	Men	26 (54.2%)	30 (44.1%)	0.286
	Women	22 (45.8%)	38 (55.9%)	
T stage (8 th)	T1	6 (12.5%)	15 (22.1%)	0.046
	T2	38 (79.2%)	39 (57.4%)	
	T3	4 (8.3%)	14 (20.6%)	
N stage (8 th)	N0	16 (33.3%)	26 (38.2%)	0.543
	N1	22 (45.8%)	33 (48.5%)	
	N2	10 (20.8%)	9 (13.2%)	
Stage (8 th)	IA	4 (8.3%)	8 (11.8%)	0.664
	IB	10 (20.8%)	12 (17.6%)	
	IIA	2 (4.2%)	6 (8.8%)	
	IIB	22 (45.8%)	33 (48.5%)	
	III	10 (20.8%)	9 (13.2%)	
PNI	Positive	42 (87.5%)	56 (82.4%)	0.590
	Negative	6 (12.5%)	11 (16.2%)	
	Unknown	0 (0%)	1 (1.5%)	
LVI	Positive	21 (43.8%)	36 (52.9%)	0.401
	Negative	27 (56.3%)	31 (45.6%)	
	Unknown	0 (0%)	1 (1.5%)	
Differentiation	WD	8 (16.7%)	2 (2.9%)	0.054
	MD	36 (75%)	56 (82.4%)	
	PD	4 (8.3%)	9 (13.2%)	
	Unknown	0 (0%)	1 (1.5%)	

Table 2. Pathological characteristics and the value of GLN 0,45,90 in pancreatic cancer patients. PNI; Perineural invasion, LVI; Lymphovascular invasion, WD; Well differentiated, MD; Moderate differentiated, PD; Poorly differentiated.

Discussion

Quantitative imaging techniques based on radiomics have recently gained prominence as potential methods to provide mineable data from imaging analysis using automatically extracted data-characterisation processes^{11–14}. CT is a good technique for assessment of the structural aspects of tumours and the normal adjacent organs. It remains the initial imaging method used for clinical staging of pancreatic cancer and for evaluating local spread into adjacent structures.

Tumour heterogeneity is a significant prognostic factor because it reflects the subclonal populations of the tumour. Tumours show temporally and spatially heterogeneous features in imaging studies (CT, MRI, and PET-CT). Since CT reflects the characteristics of these features of tumours, studies on the evaluation of tumour heterogeneity using preoperative CT scans are underway for various tumours^{15–22}. Therefore, we used CT texture analysis to determine the predictive value of preoperative CT scans in pancreatic cancer.

In this study, we analysed the differences in GLRLM values between normal pancreatic tissue and the tumours in pancreatic cancer. The GLN values were higher than normal in tumours. High GLN values represent a non-uniform texture, i.e., heterogeneity. The group with higher GLN values also showed poorer results for prognostic factors such as T stage and differentiation type. In this study, tumour heterogeneity was reflected by a high GLN value in the image and was associated with increased biological aggressiveness (higher T stage and poor differentiation of the tumour).

The biological rationale for radiologic features of heterogeneity is to determine potential histopathologic correlates (tumour grade, hypoxia, and angiogenesis-specific genetic and molecular features). Higher tumour heterogeneity, as reflected by lower uniformity of positive pixel values and greater variability in texture analysis, correlates with elevated markers of hypoxia^{23,24}.

GLN values in GLRLM features were also correlated with recurrence-free survival. GLN measures the similarity of grey level intensity values in the image, where a lower GLN value correlates with a greater similarity in intensity values. Therefore, we conclude that heterogeneity is higher in the group with GLN values greater than the median value, and that recurrence-free survival is worse than expected in this group. The GLCM value is determined only on the basis of the relationships among pixel values. Regardless of the position, heterogeneity increases as the number of pixels showing a large difference from adjacent pixels increases. However, in comparison with the GLCM, the GLRLM value is less dependent on the distribution range of pixel values in the image because the pixel values as well as the lengths of the same pixel values are considered together for GLRLM assessments²⁵.

		GLN 135		p-value
		Value < Median (n = 50)	Value > Median (n = 66)	
Age	≤65	28 (56%)	31 (47%)	0.335
	>65	22 (44%)	35 (53%)	
Sex	Men	27 (54%)	29 (43.9%)	0.283
	Women	23 (46%)	37 (56.1%)	
T stage (8 th)	T1	7 (14%)	14 (21.2%)	0.055
	T2	39 (78%)	38 (57.6%)	
	T3	4 (8%)	14(21.2%)	
N stage (8 th)	N0	17 (34%)	25 (37.9%)	0.363
	N1	22 (44%)	33 (50%)	
	N2	11 (22%)	8 (12.1%)	
Stage (8 th)	IA	5 (10%)	7 (10.6%)	0.551
	IB	10 (20%)	12 (18.2%)	
	IIA	2 (4%)	6 (9.1%)	
	IIB	22 (44%)	33 (50%)	
	III	11 (22%)	8 (12.1%)	
PNI	Positive	44 (88%)	54 (81.8%)	0.520
	Negative	6 (12%)	11 (16.7%)	
	Unknown	0 (0%)	1 (1.5%)	
LVI	Positive	22 (44%)	35 (53%)	0.394
	Negative	28 (56%)	30 (45.5%)	
	Unknown	0 (0%)	1 (1.5%)	
Differentiation	WD	8 (16%)	2 (3%)	0.081
	MD	37 (74%)	55 (83.3%)	
	PD	5 (10%)	8 (12.1%)	
	Unknown	0 (0%)	1 (1.5%)	

Table 3. Pathological characteristics and the value of GLN 135 in pancreatic cancer patients. PNI; Perineural invasion, LVI; Lymphovascular invasion, WD; Well differentiated, MD; Moderate differentiated, PD; Poorly differentiated.

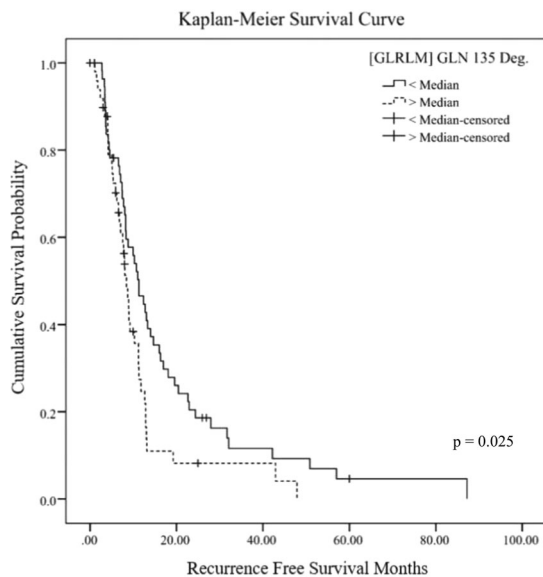


Figure 1. Kaplan Meier survival curve for recurrence-free survival according to the GLN feature (GLN135).

Most studies reporting texture analysis of tumour heterogeneity used histogram analysis and GLCM to obtain results. Although GLCM features demonstrate better performance than other texture types, the GLRLM features performed better in the optimal subset. GLCM is suitable for analysing changes in local heterogeneity because it analyses

Factors	Univariate analysis			Multivariate analysis		
	HR	95% CI	P	HR	95% CI	P
Age						
≤65	1			1		
>65	1.453	0.955–2.211	0.081	1.548	0.996–2.405	0.052
Sex						
Men	1					
Women	0.920	0.607–1.392	0.692			
T stage (8th)						
T1	1					
T2	1.316	0.723–2.398	0.369			
T3	1.891	0.864–4.139	0.111			
N stage (8th)						
N0	1			1		
N1	1.529	0.972–2.405	0.066	1.623	1.014–2.598	0.043
N2	1.574	0.784–3.158	0.202	2.804	1.319–5.957	0.007
Stage (8th)						
IA	1					
IB	0.987	0.443–2.199	0.974			
IIA	1.641	0.538–5.007	0.384			
IIB	1.619	0.781–3.354	0.195			
III	1.676	0.678–4.146	0.264			
PNI						
Positive	1					
Negative	0.851	0.470–1.541	0.594			
LVI						
Positive	1					
Negative	0.736	0.484–1.120	0.153			
Differentiation						
WD	1			1		
MD	2.238	1.071–4.676	0.032	2.309	1.072–4.976	0.033
PD	2.906	1.160–7.282	0.023	3.290	1.207–8.969	0.020
GLN0, 45, 90						
Value < median	1			1		
Value > median	1.476	0.967–2.254	0.071	0.254	0.056–1.150	0.075
GLN135						
Value < median	1			1		
Value > median	1.696	1.102–2.610	0.016	6.030	1.317–27.596	0.021

Table 4. Univariate and multivariate analyses of the relationship between RFS and clinicopathologic variables by Cox regression hazard model. PNI; Perineural invasion, LVI; Lymphovascular invasion, WD; Well differentiated, MD; Moderate differentiated, PD; Poorly differentiated, RFS; Recurrence free survival.

texture changes through the relationship between neighbouring pixels. In contrast, GLRLM is more sensitive for analysing changes in regional heterogeneity because it analyses texture changes through the entire length of the run.

Several studies have reported assessments of tumour heterogeneity by GLRLM texture analysis²⁶. For example, Ho *et al.* used GLRLM textural analysis and reported that the heterogeneity of intratumoural FDG distribution and the early temporal changes in total lesion glycolysis may be important predictors for overall survival in patients with bulky cervical cancer²⁷.

One limitation of the present study was the use of ROIs covering only the lesion core in pancreatic tumours rather than the entire tumour area or the largest cross-sectional area. In contrast, other studies performed texture analysis of the entire area²⁸. Typically, whole-tumour analysis appears to yield results that are more representative of tumour heterogeneity. However, because of the nature of tumours, proliferation usually occurs in the central part of the lesion. It is true that proliferation also occurs at the border of the tumour; however, the development of a necrotic core in cancer patients is correlated with increased tumour size, high-grade disease, and poor prognosis due to the emergence of chemoresistance and metastases²⁹. This suggests that the core of the tumour is adequate for predicting heterogeneity.

The second limitation is that this analysis did not reflect genetic heterogeneity. Biologically, to confirm tumour heterogeneity, it is essential to identify genetic heterogeneity. Without also performing genetic analysis, it is difficult to confirm that texture analysis has completely deduced the histological heterogeneity. Previous studies did not correlate pancreatic cancers with molecular markers or investigate subtypes of pancreatic cancers. However, we plan to correlate this texture analysis with genetic heterogeneity and perform genetic analysis using a prospective study design.

Factors	Univariate analysis			Multivariate analysis		
	HR	95% CI	P	HR	95% CI	P
Age						
≤65	1					
>65	1.402	0.931–2.112	0.106			
Sex						
Men	1					
Women	0.741	0.493–1.115	0.151			
T stage (8th)						
T1	1					
T2	1.321	0.748–2.332	0.337			
T3	2.195	1.086–4.435	0.028			
N stage (8th)						
N0	1					
N1	1.561	0.983–2.477	0.059			
N2	2.011	1.086–3.726	0.026			
Stage (8th)						
IA	1			1		
IB	1.094	0.457–2.619	0.840	1.133	0.472–2.720	0.780
IIA	2.169	0.776–6.064	0.140	2.397	0.832–6.909	0.105
IIB	1.888	0.890–4.006	0.098	2.346	1.094–5.029	0.028
III	2.449	1.035–5.794	0.041	3.098	1.298–7.390	0.011
PNI						
Positive	1			1		
Negative	0.542	0.279–1.052	0.070	0.450	0.221–0.916	0.028
LVI						
Positive	1					
Negative	0.714	0.474–1.075	0.107			
Differentiation						
WD	1			1		
MD	1.493	0.744–2.996	0.259	1.686	0.834–3.407	0.146
PD	1.830	0.741–4.520	0.190	3.943	1.523–10.207	0.005
GLN0, 45, 90						
Value < median	1					
Value > median	1.129	0.747–1.705	0.565			
GLN135						
Value < median	1					
Value > median	1.135	0.753–1.711	0.546			

Table 5. Univariate and multivariate analyses of the relationship between OS and clinicopathologic variables by Cox regression hazard model. PNI; Perineural invasion, LVI; Lymphovascular invasion, WD; Well differentiated, MD; Moderate differentiated, PD; Poorly differentiated, OS; Overall survival.

Inferring tumour heterogeneity through texture analysis, a radiomics approach, has several advantages and disadvantages. We have identified a tool for prediction of the postoperative oncologic outcome and prognosis through preoperative abdominal CT scans in aggressive cancers such as pancreatic cancer.

No previous studies have reported resectable pancreatic cancers with the same adjuvant treatments, and the present study had a larger sample size than previous studies. Our study has great significance as we performed the same texture analysis with a different method^{30,31}.

Despite the fact that this study used retrospective data, our result may indicate an important predictor of prognosis, since we used the preoperative CT scan of resectable pancreatic cancer patients.

In conclusion, the findings obtained with texture analysis show clinical significance in predicting the survival and prognosis of pancreatic cancer patients.

Methods

Patients. We included 230 consecutive patients who underwent curative-intent surgical resection for pancreatic cancer at Gangnam Severance Hospital between 2001–2017. Preoperative contrast-enhanced CT data of 116 patients were available for texture analysis. Patients who had undergone neoadjuvant concurrent chemoradiotherapy were excluded from this analysis. The study protocol was approved by the institutional review board at Gangnam Severance Hospital, Yonsei University of Korea (3-2016-0338). The study complied with the Declaration of Helsinki. Informed consent was obtained from all participants.



Figure 2. ROI processing in preoperative CT scan.

CT protocol. For the 116 patients, preoperative dynamic CT was performed using one of two scanners: a 16-slice multidetector CT (MDCT) scanner (Somatom Sensation 16; Siemens Medical Solutions, Erlangen, Germany) or a 64-slice MDCT scanner (Somatom Sensation 64; Siemens Medical Solutions, Erlangen, Germany). All patients were instructed to fast for at least 5 hours before undergoing CT examinations. Each patient was administered 150 mL of a nonionic contrast material (Ultravist 300; Schering AG, Berlin, Germany) intravenously by means of a power injector (EnVision CT; Medrad, Pittsburgh, Pa) at a rate of 3 mL/second.

The CT images were acquired in the craniocaudal direction with the following parameters: detector collimation, 16×0.75 mm; table feed, 12 mm per rotation; section width, 3 mm; reconstruction increment, 3 mm with 3-mm-thick sections; pitch, 1.2; tube voltage, 120 kVp; and tube current, 160 mAs. Precontrast scanning (i.e., the first pass) was performed first, followed by contrast-enhanced CT. In order to determine the time of peak aortic enhancement, a bolus injection of 20 mL of contrast material was administered, and sequential dynamic sections were acquired every 2 seconds, starting from the hepatic hilum. Based on the findings of a previous study on multidetector row helical CT, we calculated the start time for the arterial phase by adding 15 seconds to the time of peak aortic enhancement calculated at the hepatic hilum. The resultant average start time for the arterial phase was 34 seconds (range, 30 ± 38 seconds). The equilibrium phase scan was acquired at 3 minutes after the start of the contrast material injection³².

Data analysis. For each primary cancer site, a region of interest (ROI) was drawn on all slices with a visible tumour on the AP CT scans using the GCUBME-ROI Tool. This tool is a program created independently for this study. The ROIs were reviewed by a radiologist blinded to the patient outcomes. The circular ROI was placed within the central region of the tumour and the normal parenchyma in the pancreas without including the pancreatic and bile ducts and vessels. All ROIs had the same diameter (4 mm) (Fig. 2).

Texture analysis. For texture analysis, pixel values in the ROIs were transformed into the GLRLM matrix for each CT image. GLRLM provides the size of homogeneous runs for each grey level along a specific linear direction, which is defined by four different directions in the 2D GLRLM, i.e., 0° , 45° , 90° , and 135° . In the GLRLM matrix, the rows are represented by grey values, and the columns are represented by the number of same adjacent pixels. The grey-level non-uniformity (GLN) features were calculated from the GLRLM matrix for the four directions using Eq. (1):

$$\sum_{i=0}^{G-1} \left(\sum_{j=0}^{R-1} P_{i,j} \right)^2 \quad (1)$$

GLN measures the distribution of runs along the grey levels. The GLN feature value is low when the runs are equally distributed along grey levels. Therefore, a low GLN feature value indicates high similarity of intensity values. In the GLRLM matrix, the rows are represented by grey values, and the columns are expressed by the same number of adjacent pixels^{25,33}. The number of occurrences wherein the grey value of each of the pixels is the same as the grey value of the neighbouring pixels in a given direction and distance is represented by a matrix.

Statistical analysis. All statistical analyses were performed using SPSS software, version 20.0 (SPSS Inc., Chicago, IL). Categorical variables were evaluated using chi-square or Fisher's exact tests. Survival curves were plotted using the Kaplan–Meier method, and intergroup differences in survival time were assessed with the log-rank test. Recurrence-free survival was defined as the interval between the date of surgery and the date of recurrence. The Cox proportional hazards regression method was used to determine independent prognostic factors. A p-value lower than 0.05 was considered statistically significant.

Received: 14 February 2019; Accepted: 6 November 2019;

Published online: 22 November 2019

References

1. Siegel, R., Ward, E., Brawley, O. & Jemal, A. Cancer statistics, 2011: the impact of eliminating socioeconomic and racial disparities on premature cancer deaths. *CA Cancer J Clin.* **61**, 212–236 (2011).
2. Kleeff, J. *et al.* Surgery for recurrent pancreatic ductal adenocarcinoma. *Ann Surg.* **245**, 566–572 (2007).
3. Aerts, H. J. W. L. *et al.* Decoding tumour phenotype by noninvasive imaging using a quantitative radiomics approach. *Nature Communications.* **5**, 4006, <https://doi.org/10.1038/ncomms5006> (2014).
4. Davnall, F. *et al.* Assessment of tumor heterogeneity: an emerging imaging tool for clinical practice? *Insights Imaging.* **3**, 573–589 (2012).
5. Yip, C. *et al.* Assessment of changes in tumor heterogeneity following neoadjuvant chemotherapy in primary esophageal cancer. *Diseases of the Esophagus.* **28**, 172–179 (2015).
6. Yang, F., Thomas, M. A., Dehdashti, F. & Grigsby, P. W. Temporal analysis of intratumoral metabolic heterogeneity characterized by textural features in cervical cancer. *European Journal of Nuclear Medicine and Molecular Imaging.* **40**, 716–727 (2013).
7. Win, T. *et al.* Tumor Heterogeneity and Permeability as Measured on the CT Component of PET/CT Predict Survival in Patients with Non-Small Cell Lung Cancer. *Clinical Cancer Research.* **19**, 3591–3599 (2013).
8. Liu, Y. *et al.* Tumor heterogeneity assessed by texture analysis on contrast-enhanced CT in lung adenocarcinoma: association with pathologic grade. *Oncotarget.* **8**, 53664–53674 (2017).
9. Chakraborty, J. *et al.* Preliminary study of tumor heterogeneity in imaging predicts two year survival in pancreatic cancer patients. *PLoS One.* **12**, e0188022, <https://doi.org/10.1371/journal.pone.0188022> (2017).
10. Greene, F. L. *AJCC Cancer Staging Manual Eighth Edition.* 337–347 (2016)
11. Kumar, V. *et al.* Radiomics: the process and the challenges. *Magnetic Resonance Imaging.* **30**, 1234–1248 (2012).
12. Lambin, P. *et al.* Radiomics: Extracting more information from medical images using advanced feature analysis. *European Journal of Cancer.* **48**, 441–446 (2012).
13. Larue, R. T. H. M., Defraene, G., De Ruyscher, D., Lambin, P. & Van Elmpt, W. Quantitative radiomics studies for tissue characterization: a review of technology and methodological procedures. *British Journal of Radiology.* **90**, 1070, <https://doi.org/10.1259/bjr.20160665> (2017).
14. Parmar, C. *et al.* Robust Radiomics Feature Quantification Using Semiautomatic Volumetric Segmentation. *Plos One.* **9**, e102107, <https://doi.org/10.1371/journal.pone.0102107> (2014).
15. Ganeshan, B., Skogen, K., Pressney, I., Coutroubis, D. & Miles, K. Tumour heterogeneity in oesophageal cancer assessed by CT texture analysis: Preliminary evidence of an association with tumour metabolism, stage, and survival. *Clinical Radiology.* **67**, 157–164 (2012).
16. Lu, L. C., Hsu, C. H., Hsu, C. & Cheng, A. L. Tumor Heterogeneity in Hepatocellular Carcinoma: Facing the Challenges. *Liver Cancer.* **5**, 128–138 (2016).
17. Lubner, M. G., Stabo, N., Abel, E. J., Del Rio, A. M. & Pickhardt, P. J. CT Textural Analysis of Large Primary Renal Cell Carcinomas: Pretreatment Tumor Heterogeneity Correlates With Histologic Findings and Clinical Outcomes. *AJR Am J Roentgenol.* **207**, 96–105 (2016).
18. Mu, W. *et al.* Staging of cervical cancer based on tumor heterogeneity characterized by texture features on (18)F-FDG PET images. *Phys Med Biol.* **60**, 5123–5139 (2015).
19. Ng, F., Ganeshan, B., Kozarski, R., Miles, K. A. & Goh, V. Assessment of Primary Colorectal Cancer Heterogeneity by Using Whole-Tumor Texture Analysis: Contrast-enhanced CT Texture as a Biomarker of 5-year Survival. *Radiology.* **266**, 177–184 (2013).
20. Anishiyi, P. & Sasikala, M. Statistical texture feature set based classification of histopathological images of stomach adenocarcinoma. *Biomedical Research-India.* **27**, S80–S86 (2016).
21. Hanania, A. N. *et al.* Quantitative imaging to evaluate malignant potential of IPMNs. *Oncotarget.* **7**, 85776–85784 (2016).
22. Lee, H. S. *et al.* Differentiating the grades of thymic epithelial tumor malignancy using textural features of intratumoral heterogeneity via F-18-FDG PET/CT. *Annals of Nuclear Medicine.* **30**, 309–319 (2016).
23. Ganeshan, B. & Miles, K. A. Quantifying tumour heterogeneity with CT. *Cancer Imaging.* **13**, 140–149 (2013).
24. Ganeshan, B. *et al.* Non-small cell lung cancer: histopathologic correlates for texture parameters at CT. *Radiology.* **266**, 326–336 (2013).
25. Loh, H. H., Leu, J. G. & Luo, R. C. The Analysis of Natural Textures Using Run Length Features. *Ieee Transactions on Industrial Electronics.* **35**, 323–328 (1988).
26. Liu, Y. *et al.* Relationship between Glioblastoma Heterogeneity and Survival Time: An MR Imaging Texture Analysis. *American Journal of Neuroradiology.* **38**, 1695–1701 (2017).
27. Ho, K. C. *et al.* A preliminary investigation into textural features of intratumoral metabolic heterogeneity in F-18-FDG PET for overall survival prognosis in patients with bulky cervical cancer treated with definitive concurrent chemoradiotherapy. *American Journal of Nuclear Medicine and Molecular Imaging.* **6**, 166–75 (2016).
28. Ng, F., Kozarski, R., Ganeshan, B. & Goh, V. Assessment of tumor heterogeneity by CT texture analysis: Can the largest cross-sectional area be used as an alternative to whole tumor analysis? *European Journal of Radiology.* **82**, 342–348 (2013).
29. Lee, S. Y. *et al.* Regulation of Tumor Progression by Programmed Necrosis. *Oxid Med Cell Longev.* **2018**, 3537471, <https://doi.org/10.1155/2018/3537471> (2018).
30. Yun, G. *et al.* Tumor heterogeneity of pancreas head cancer assessed by CT texture analysis: association with survival outcomes after curative resection. *Sci Rep.* **8**, 7226, <https://doi.org/10.1038/s41598-018-25627-x> (2018).
31. Eilaghi, A. *et al.* CT texture features are associated with overall survival in pancreatic ductal adenocarcinoma - a quantitative analysis. *BMC Med Imaging.* **17**, 38, <https://doi.org/10.1186/s12880-017-0209-5> (2017).
32. Kang, J. H. *et al.* Prediction of pancreatic fistula after pancreatoduodenectomy by preoperative dynamic CT and fecal elastase-1 levels. *PLoS One.* **12**, e0177052, <https://doi.org/10.1371/journal.pone.0177052> (2017).
33. Tang, X. Texture Information in Run-Length Matrices. *IEEE Transactions On Image Processing.* **7**, 1602–1609 (1998).

Acknowledgements

We have no funding for our research.

Author contributions

Study design: Joon Seong Park, Kwang Gi Kim. Data collections: Hyung Sun Kim, Young Jae Kim. Data analysis: Hyung Sun Kim, Young Jae Kim. Writing - original draft: Hyung Sun Kim. Writing - review and editing: Joon Seong Park, Kwang Gi Kim.

Competing interests

The authors declare no competing interests.

Additional information

Correspondence and requests for materials should be addressed to K.G.K. or J.S.P.

Reprints and permissions information is available at www.nature.com/reprints.

Publisher's note Springer Nature remains neutral with regard to jurisdictional claims in published maps and institutional affiliations.



Open Access This article is licensed under a Creative Commons Attribution 4.0 International License, which permits use, sharing, adaptation, distribution and reproduction in any medium or format, as long as you give appropriate credit to the original author(s) and the source, provide a link to the Creative Commons license, and indicate if changes were made. The images or other third party material in this article are included in the article's Creative Commons license, unless indicated otherwise in a credit line to the material. If material is not included in the article's Creative Commons license and your intended use is not permitted by statutory regulation or exceeds the permitted use, you will need to obtain permission directly from the copyright holder. To view a copy of this license, visit <http://creativecommons.org/licenses/by/4.0/>.

© The Author(s) 2019